Whole-Body Distribution and Brain Tumor Imaging with ^{11}C-4DST: A Pilot Study

Jun Toyohara[1], Tadashi Nariai[2], Muneyuki Sakata[1], Keiichi Oda[1], Kenji Ishii[1], Takuya Kawabe[3], Toshiaki Irie[4], Tsuneo Saga[4], Kazuo Kubota[5], and Kiichi Ishiwata[1]

[1]Positron Medical Center, Tokyo Metropolitan Institute of Gerontology, Tokyo, Japan; [2]Department of Neurosurgery, Tokyo Medical and Dental University, Tokyo, Japan; [3]Katsuta Hospital Mito Gamma House, Mito, Japan; [4]Molecular Imaging Center, National Institute of Radiological Sciences, Chiba, Japan; and [5]Department of Radiology, National Center for Global Health and Medicine, Tokyo, Japan

Recently, we developed [methyl-^{11}C]4′-thiothymidine (^{11}C-4DST) as an in vivo cell proliferation marker. The present study was performed to determine the safety, distribution, radiation dosimetry, and initial brain tumor imaging of ^{11}C-4DST in humans. **Methods:** Multiorgan biodistribution and radiation dosimetry of ^{11}C-4DST were assessed in 3 healthy humans, who underwent 2-h whole-body PET scanning. Radiation dosimetry was estimated from the residence times of source organs using the OLINDA program. Six brain tumor patients underwent dynamic ^{11}C-4DST scans with arterial blood sampling. These patients were also evaluated with ^{11}C-methionine PET on the same day ($n = 4$) as, or 3 wk before ($n = 2$), ^{11}C-4DST PET studies. Metabolites in plasma and urine samples were analyzed by high-performance liquid chromatography. Breakdown of the blood–brain barrier in tumor tissue was confirmed by gadolinium-enhanced T1-weighted MRI. **Results:** There were no serious adverse events in any subjects at any time during the study period. ^{11}C-4DST PET demonstrated selective uptake in the bone marrow, which has a high rate of proliferation. In addition, high-level uptake was also seen in the liver. The highest absorbed organ dose was in the urinary bladder wall (17.6 μGy/MBq). The estimated effective dose for ^{11}C-4DST was 4.2 μSv/MBq. ^{11}C-4DST showed little uptake in normal brain tissues, resulting in low background activity for imaging of brain tumors. In contrast, ^{11}C-4DST PET demonstrated rapid uptake in aggressive tumor masses, whereas no signal of ^{11}C-4DST was seen in clinically stable disease in which ^{11}C-methionine uptake was high. The distribution pattern of ^{11}C-methionine in tumor regions was not always identical to that of ^{11}C-4DST. Analysis of plasma samples by high-performance liquid chromatography indicated that more than 60% of the radioactivity was present as unchanged ^{11}C-4DST at 20 min. **Conclusion:** The initial findings of the present study in a small group of patients indicated that ^{11}C-4DST PET is feasible for imaging of brain tumors. Dosimetry and pharmacologic safety were acceptable at the dose required for adequate PET images.

Key Words: 4DST; dosimetry; brain tumor; cell proliferation

J Nucl Med 2011; 52:1322–1328
DOI: 10.2967/jnumed.111.088435

Increased cell proliferation is an integral part of the cancer phenotype. In addition, the DNA incorporation method with [^{3}H-methyl]-thymidine is considered the gold standard for characterizing cell proliferation. Therefore, imaging of cell proliferation has long been a goal of nuclear medicine, and a great deal of research effort has focused on the development of radiotracers for DNA synthesis (*1,2*). In the 1970s, ^{11}C-thymidine was first advocated for PET imaging of cell proliferation (*3*). However, the issues of tracer (nucleoside) degradation in vivo were largely unrealized and not addressed. In contrast, extensive developments in the 1990s and early 2000s led to validation studies that yielded a multicompartment, metabolite-corrected kinetic model of image data for 2-^{11}C-thymidine in somatic and brain tumors that can be used to estimate thymidine flux (i.e., 1-way net clearance) from blood into DNA (*4–7*). From these investigations, it became clear that the accurate interpretation of ^{11}C-thymidine PET requires enormous labor for both patients and physicians: multiple injections of different tracers (^{11}C-CO$_2$ and ^{11}C-thymidine), arterial blood sampling, several different metabolites, and complex data analysis. Moreover, the short physical half-life of ^{11}C and difficulty of its synthesis limited the routine use of ^{11}C-thymidine for clinical imaging. Since then, several attempts have been made to find suitable thymidine analogs that can be labeled more easily with radionuclides and are resistant to degradation in vivo (*1,2*). Among the analogs reported to date, 3′-deoxy-3′-^{18}F-fluorothymidine has been selected as the most promising tracer (*8*). Unlike thymidine, 3′-deoxy-3′-^{18}F-fluorothymidine is not incorporated into DNA because it lacks 3′-hydroxyl.

Alternatively, we developed [methyl-^{11}C]4′-thiothymidine (^{11}C-4DST) as a new candidate for cell proliferation imaging (*9,10*). ^{11}C-4DST is resistant to degradation by thymidine

---

Received Jan. 23, 2011; revision accepted Apr. 7, 2011.

For correspondence or reprints contact: Jun Toyohara, Positron Medical Center, Tokyo Metropolitan Institute of Gerontology, 1-1 Naka-cho, Itabashi-ku, Tokyo 173-0022, Japan.
E-mail: toyohara@pet.tmig.or.jp

phosphorylase and incorporated into DNA. Although the short physical half-life of ^{11}C places a significant limitation on counting statistics and on commercial convenience for widespread routine clinical use, it has benefits with regard to lower radiation burden, diagnosis using multiple tracers such as ^{18}F-FDG and ^{11}C-methionine, and repeated scanning during the course of therapy. For this reason, there is a significant opportunity for the use of ^{11}C-4DST in several clinical settings, and this opportunity prompted us to undertake the first clinical trials of ^{11}C-4DST.

Here, we report the safety, radiation dosimetry, and initial brain tumor imaging of ^{11}C-4DST in humans.

MATERIALS AND METHODS

General

4DST and its precursor, 5-tributylstannyl-4′-thio-2′-deoxyuridine, were prepared by a method described previously (*9*). All chemical reagents were obtained from commercial sources. The study protocol was approved by our Institutional Review Board. Written informed consent was obtained from each subject after the procedures had been fully explained.

Preparation of ^{11}C-4DST

Carbon methylation of the precursor via a palladium-mediated Stille cross-coupling reaction with ^{11}C-methyl iodide was performed by a slight modification of a previously described procedure (*10,11*). Details on the method, results, and quality control data of ^{11}C-4DST preparation are provided in the supplemental materials (supplemental materials are available online only at http://jnm.snmjournals.org).

Subjects

Three healthy male volunteers and 6 patients with brain tumors were enrolled in this study (Table 1). The 3 volunteers (subjects 7−9; age, 21 y; mean weight (±SD), 65.2 ± 18.8 kg; weight range, 49.6–86.0 kg) participated in the whole-body distribution study. They were free of somatic and neuropsychiatric illnesses, according to medical history and physical examination findings. The 6 patients (subjects 1−6; mean age, 48.7 ± 7.1 y; age range, 42–62 y; mean weight, 64.4 ± 7.5 kg; weight range, 51.3–70.8 kg) were 4 men and 2 women who were recruited for the dynamic brain PET study. Three had grade 3 astrocytoma, 1 had grade 3 oligodendroglioma, 1 had a metastatic brain tumor of lung cancer origin, and 1 had malignant lymphoma. All malignant brain tumors were graded according to the World Health Organization scheme. Five of the 6 patients were included in the safety monitoring of ^{11}C-4DST.

Because ^{11}C-4DST does not cross the intact blood–brain barrier, all patients underwent standard gadolinium-enhanced T1-weighted MRI (Gd-MRI) of the brain to confirm breakdown of the blood–brain barrier in tumor tissues before PET. Clinical data for each patient were collected on standardized forms that included detailed initial and follow-up information.

Safety Monitoring

For 5 patients, safety data were collected after administration of ^{11}C-4DST and throughout the 1-wk follow-up period. Safety monitoring included the recording of adverse events, changes in vital signs, physical examination findings, electrocardiogram findings, and laboratory parameters (results of serum biochemistry and hematology analysis). Vital signs, including blood pressure, temperature, and respiratory rate, were monitored and recorded closely during ^{11}C-4DST imaging procedures at baseline, during ^{11}C-4DST injection, during the PET scan at 20, 40, and 60 min, and then within approximately 1 h after the PET scan. The electro-

TABLE 1
Subject Characteristics, Pretreatment, and ^{11}C-4DST PET Protocol and Data

					Protocol			Data		
Subject no.	Age (y)	Sex	Diagnosis	Pretreatment	Region	Dose (MBq/nmol)	Duration (min)	Mean SUV	Maximal SUV	*K*i (min^{-1})
1	42	M	Oligo (grade 3)	Op/XRT (55 Gy)/TMZ	Brain	528/1.7	45	2.2	3.3	0.047
					C/L brain			0.5	1.0	0.010
2	48	M	As (grade 3)	XRT (60 Gy)/TMZ/GK	Brain	745/10.0	60	0.8	1.6	—*
					C/L brain			0.3	0.8	—*
3	56	M	As (grade 3)	Op/GK/TMZ	Brain	749/2.5	90	0.9	1.2	0.017
					C/L brain			0.3	0.6	0.007
4	44	M	As (grade 3)	—	Brain	731/3.8	90	1.3	2.3	0.025
					C/L brain			0.6	1.5	0.011
5	46	F	Lym	—	Brain	727/5.9	40	1.2	2.4	0.044
					C/L brain			0.5	1.0	0.015
6	50	F	Met (from LK)	Op/GK (×3)	Brain	817/1.9	60	2.1	5.1	0.046
					C/L brain			0.5	0.8	0.010
7	21	M	Normal	—	Whole body	655/11.4	120		—	—
8	21	M	Normal	—	Whole body	743/9.5	120		—	—
9	21	M	Normal	—	Whole body	666/7.7	120		—	—

**K*i calculation was excluded because of failure of arterial blood sampling.

Oligo = oligodendroglioma; op = surgical operation; TMZ = temozolomide; C/L brain = contralateral normal brain; as =astrocytoma; XRT = external-beam radiotherapy; GK = γ-knife surgery; lym = malignant lymphoma; met = metastasis; LK = lung carcinoma.

Mean SUV was for 45 to 60 min after injection of ^{11}C-4DST, except in subjects 1 (30−45 min) and 5 (30−40 min).

cardiogram was recorded continuously starting before the ^{11}C-4DST injection and continuing throughout the whole imaging procedure. Blood samples were obtained at baseline in all patients and 1 wk after radioligand administration in 3 patients. The following blood assays were performed: sodium, potassium, chloride, calcium, and glucose levels; hepatic function assays (aspartate aminotransferase, alanine aminotransferase, alkaline phosphatase, lactate dehydrogenase, cholinesterase, and total protein); creatinine and blood urea nitrogen; amylase and creatine kinase; lipid metabolism (total cholesterol and triglyceride); and a hematologic evaluation consisting of a complete blood count, including red blood cell count, hematocrit, hemoglobin, white blood cell count, differential leukocyte count, and platelet count.

Whole-Body Imaging

The protocol for investigating radiation dosimetry in humans using whole-body imaging was essentially the same as that reported previously (*12*). Whole-body PET scans were obtained using SET-2400W (Shimadzu) in 2-dimensional mode. This scanner has an axial field of view of 20 cm and acquires 63 slices at a center-to-center interval of 3.125 mm (*13*). Before the ^{11}C-4DST was injected, the subjects were asked to void their bladders. Whole-body emission scanning was performed, with 7 frames (~125 min in total) obtained starting 1 min after intravenous bolus injection of 688 ± 47.9 MBq of ^{11}C-4DST. Each frame covered the body from the head to the urinary bladder and consisted of 5 bed positions. The duration of scanning at each bed position was increased to compensate for the short half-life of ^{11}C: 120 s/bed position for frames 1–3, 240 s/bed position for frames 4–6, and 360 s/bed position for the last frame. At the last frame, transmission data with a rotating ^{68}Ge/^{68}Ga line source to correct for attenuation were acquired simultaneously (*14*). The sum of intervals for the moving bed was approximately 90 s/frame. After the dynamic PET procedure, the subjects were asked to urinate again, and the radioactivity of the urine was measured using a radioisotope calibrator (CRC-712; Capintec). Radioactive metabolites in the urine were analyzed by high-performance liquid chromatography (HPLC). Images were reconstructed with ordered-subset expectation maximization followed by application of a gaussian postprocessing filter of 6 mm in full width at half maximum. The resulting images were 128 × 128 × 25 voxels for each bed position (voxel size, 4 × 4 × 6.25 mm). Regions of interest (ROIs) were placed over 9 organs that could be identified: lungs, heart wall, liver, spleen, bone marrow (thoracic and lumbar vertebrae), small intestine, kidneys, muscle (psoas major muscle), and urinary bladder. The decay-uncorrected and decay-corrected time–activity curves of organs were calculated as the percentage of the injected dose per organ or as a standardized uptake value (SUV): (activity/mL of tissue)/(injected activity/g of body weight). For organs that were measured in 2 split images of different bed positions, the data of each bed position were included in the time course as discrete time points. Residence time, in hours, for all source organs is equal to the area under the time course curve multiplied by the volume of the organ ROI. The volume of bone marrow, in which only part of the organ could be measured, was substituted by a volume calculated from the mass of red marrow in the adult male phantom (1.12 kg for a 73.7-kg body) adjusted by the subject's body weight and using 1 g/mL as the specific gravity (*15*). The radioactivity in the muscle was combined into the background (remainder-of-body) activity. The area under the time course curve was calculated by summing the area from time 0 to the endpoint of the scan and the area from the endpoint of the scan to infinity. The former area was calculated by trapezoidal integration. The latter area was calculated by integration of a monoexponential curve passing through the final 2 scan points.

The absorbed dose in 25 target organs of the adult male phantom was estimated from the residence times of source organs by implementing the MIRD method using OLINDA (Vanderbilt University) (*16*). The effective dose was also calculated by OLINDA using the methodology described in International Commission on Radiological Protection Publication 60 (*17*).

Brain PET

^{11}C-4DST PET was performed using the SET-2400W scanner. After transmission scanning with a rotating ^{68}Ga/^{68}Ge line source to correct for attenuation, ^{11}C-4DST (528–817 MBq/1.7–10.0 nmol) was injected intravenously for 1 min into each patient, and then dynamic PET (45–90 min) with 2-dimensional acquisition (10 s × 6 frames, 30 s × 3 frames, 60 s × 5 frames, 150 s × 5 frames, and 300 s × 14 frames in a 90-min scan) was performed. After the dynamic scan, urine was recovered from the patients. Earlier on the same day ($n = 4$) or within 3 wk before ($n = 2$) the ^{11}C-4DST scan, the ^{11}C-methionine PET scan was performed as described previously (*18*). PET with 3-dimensional acquisition was performed by measuring the equilibrated radioactivity 20 min after intravenous ^{11}C-methionine injection (~300 MBq). The 2 radioligand injections were separated by more than 2 h to allow for decay of radioactivity. For ^{11}C-4DST PET scans, arterial blood was sampled at 10, 20, 30, 40, 50, 60, 70, 80, 90, 100, 110, 120, 135, 150, and 180 s, as well as at 5, 7, 10, 15, 20, 30, 40, 50, 60, 75, and 90 min (in a 90-min scan), the whole blood and separated plasma were weighed, and radioactivity was measured with a NaI (Tl) well scintillation counter. To analyze the labeled metabolites, 1 mL of additional blood was obtained at 3, 10, 20, 30, 40, and 60 min. Unaltered ^{11}C-4DST in the plasma was analyzed by HPLC, and the metabolite-corrected time–activity curve of plasma was obtained.

Tomographic images were reconstructed using a filtered backprojection method with a cutoff frequency of 1.25 cycles/cm and order 2. The data were collected in a 128 × 128 × 31 matrix, and the voxel size was 2 × 2 × 6.25 mm. The ^{11}C-methionine image and Gd-MRI scan were registered to the ^{11}C-4DST image based on normalized mutual information. ROIs were placed manually over tumor and control brain regions on the ^{11}C-4DST image with reference to the Gd-MRI scan and ^{11}C-methionine image. Partially overlapping circular 10-mm-diameter ROIs were placed on the area of maximum ^{11}C-4DST uptake in a lesion on consecutive transaxial slices or the area of maximum ^{11}C-methionine uptake if increased ^{11}C-4DST uptake was absent. The control ROIs were placed on corresponding contralateral regions. The volumes of these ROIs were 1.5–10 mL, depending on the tumor size. Time–activity curves for these ROIs were calculated as Bq/mL or as SUV. Using the time–activity curves of tissues and the metabolite-corrected time–activity curve of plasma, the rate constant Ki (min^{-1}) (net irreversible retention of the radioligand within the imaging time) of ^{11}C-4DST was estimated by Patlak plot graphical analysis (quasi-steady state was reached at 10 min) (*19*).

Metabolite Analysis

Metabolites of ^{11}C-4DST in the plasma sampled at 3, 10, 20, 30, 40, and 60 min and in urine recovered at 55–132 min were analyzed by HPLC. The blood was centrifuged at 7,000*g* for 1 min at 4°C to obtain the plasma, which was denatured with 2 volumes of 7.5% trichloroacetic acid in an ice-water bath. The suspension was centrifuged under the same conditions and divided into acid-soluble and acid-precipitable fractions. The precipitate was resuspended in 0.5 mL of 5% trichloroacetic acid followed by centrifugation. This procedure was repeated twice. Radioactivity in the 3 acid-soluble fractions and precipitates was measured with an auto-γ-counter (Wallac). In this treatment of plasma, less than 1% of the total radioactivity was left in the final precipitates. The acid-soluble fractions were combined, and after centrifugation of the samples, the supernatant was analyzed by HPLC with a radioactivity detector (FLO-ONE 150TR; Packard Instruments). A YMC-Pack ODS-A column (10 × 150 mm; YMC) was used with acetonitrile/50 mM aqueous acetic acid/50 mM aqueous sodium acetate, pH 4.5 (9.7/45.15/45.15, v/v/v) at a flow rate of 2 mL/min. The retention time of ^{11}C-4DST was 6.5 min. The recovery in the eluate of the injected radioactivity was essentially quantitative.

In the case of urine, the sample was directly applied to HPLC. Two urine samples were further treated with β-glucuronidase type HP-2 from *Helix pomatia* (Sigma-Aldrich) as described previously with slight modifications (*20*). Briefly, urine samples were adjusted to pH 5.0 with 2 M HCl. Then, 0.25 mL of this urine was mixed with 50 μL of 1 M sodium acetate buffer (pH 4.5) and 5 μL of β-glucuronidase (520 units of β-glucuronidase activity and 4.2 units of sulfatase activity). The reaction mixture was incubated for 1 h at 37°C and then denatured with an equal volume of 10% trichloroacetic acid following the same procedure as described for plasma sample preparation.

RESULTS

Safety Monitoring

Table 1 shows the injected radioactivity (MBq) and dose (nmol) of ^{11}C-4DST for each subject. Administration of ^{11}C-4DST was well tolerated by all subjects. No drug-related adverse events were reported for patients in this study. No clinically important trends indicative of a safety signal were noted for laboratory parameters, vital signs, or electrocardiogram parameters. Transient asymptomatic increases in blood pressure were observed in subjects 3 and 6 (from 96/62 to 134/67 and from 122/74 to 144/90, respectively) after PET. This was attributable to discomfort from the head immobilization device, positioning, and the need to hold still for the long period of the examination.

Whole-Body Imaging

The whole-body distribution of ^{11}C-4DST in subject 8 is shown in Figure 1. Figure 2 shows typical decay-corrected time–activity curves for the same subject. In the first frame, the kidney showed the highest uptake of radioactivity, which rapidly decreased thereafter. The urinary bladder showed an accumulation of radioactivity corresponding to radioactivity clearance by the kidneys. The mean radioactivity voided into urine was 13.9% ± 1.7% of the injected activity. ^{11}C-4DST PET also showed the second highest uptake of radioactivity in the liver at the first frame, followed by a gradual decrease. Bone marrow showed a gradual increase in radioactivity, and the second highest level of radioactivity uptake was seen in the last frame, which indicated selective uptake of ^{11}C-4DST in tissues with a high rate of proliferation in humans. Moderate ^{11}C-4DST uptake was also observed in the proliferating tissues, such as the spleen and small intestine. We could not identify any reversible loss of radioactivity in these proliferating tissues during the 120-min scan. Nonproliferating tissues, such as muscle and lungs, showed the lowest uptake. The residence times are shown in Supplemental Table 1, and the organ-absorbed and effective doses are shown in Table 2. The highest absorbed dose was observed in the urinary bladder wall, followed by the kidneys, liver, and spleen. The mean estimated effective dose was 4.2 ± 0.3 μSv/MBq.

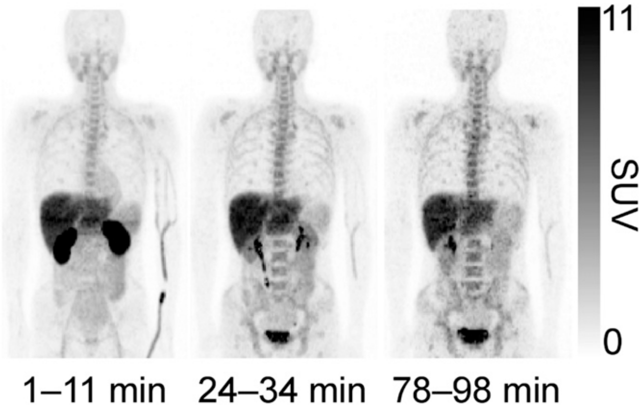

FIGURE 1. Representative whole-body decay-corrected maximum-intensity-projection images of ^{11}C-4DST (subject 8) after intravenous injection of ^{11}C-4DST.

Brain PET

The scan duration, mean SUV, maximal SUV, and *K*i are summarized in Table 1. The scan duration was variable (40−90 min) because the patients had varied indications for imaging. Subjects 1−3 and 6 were treated previously with multidisciplinary therapy, and the other 2 subjects (4 and 5) had newly identified tumors. In all patients, tumor masses were serially monitored with Gd-MRI or ^{11}C-methionine PET. ^{11}C-4DST showed little uptake in the normal brain, resulting in low background activity for imaging of brain tumors (Fig. 3). Physiologic uptake was observed in salivary glands and proliferating tissues, nasal mucosa, and bone marrow. Tumors in newly identified or aggressively growing masses confirmed by serial Gd-MRI were clearly visualized by ^{11}C-4DST (Fig. 3; all subjects except subject 3). In contrast, a clinically stable tumor mass confirmed by serial Gd-MRI was not visualized by ^{11}C-4DST PET (Fig. 3; subject 3). ^{11}C-methionine PET visualized all Gd-MRI contrast-enhanced regions. The distribution pattern of ^{11}C-methionine in tumor regions was not identical to that of ^{11}C-4DST even in the ^{11}C-4DST–positive tumor masses (Fig. 3).

Supplemental Figure 1 shows representative decay-corrected time–activity curves of brain tumors. One patient (subject 2) was excluded from the calculation of *K*i because of failure of arterial blood sampling. The time–activity curves of each tumor region were variable, suggesting heterogeneity of

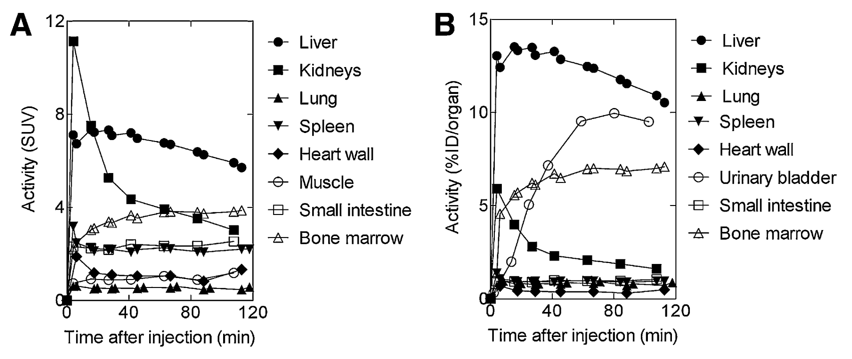

FIGURE 2. Regional decay-corrected time–activity curves after intravenous injection of ^{11}C-4DST in same subject as shown in Figure 1: SUV of source organs (A) and percentage injected dose (%ID) per source organ (B).

tumor proliferation between tumor masses. The time–activity curves of subjects 5 and 6 showed continuous accumulation of radioactivity over the first 20 min and then reached a plateau, indicating a pattern of accumulation with no washout (Supplemental Figs. 1D and 1E). On the other hand, the time–activity curve of subject 4 decreased gradually after an initial increase and then approached a plateau, indicating a washout pattern (Supplemental Fig. 1C). The time–activity curves of subjects 1 and 2 (data not shown) were between those of subjects 4 and 6 (Supplemental Fig. 1A). The plateau level of radioactivity in each tumor mass suggested that elimination of radioactive metabolites from the tumor tissues was negligible during the study. In contrast, the time–activity curve of clinically stable subject 3 gradually decreased after an initial low level of radioactivity and still decreased during the course of the study (Supplemental Fig. 1B). Representative Patlak plots for tumor masses and contralateral normal brain regions are shown in Supplemental Figure 2A (subject 4). A discernible linear phase was seen at 10–40 min ($n = 1$), 10–45 min ($n = 1$), 10–60 min ($n = 1$), and 10–90 min ($n = 2$) after injection; Ki was higher in tumor tissue than in normal brain tissues. The Ki values corresponded well to the SUV (Supplemental Fig. 2B).

Metabolite Analysis

The results of HPLC analysis of plasma are summarized in Table 3. Parent activity was eluted at a retention time of approximately 6.5 min. ^{11}C-4DST was metabolized to hydrophilic metabolites, and at least 5 radioactive metabolites were detected between the elution front (2.5 min) and 5 min on the chromatogram (M1; 2.5 min, M2; 3.0 min, M3; 4.0 min, M4; 4.5 min, and M5; 5.0 min). At 60 min after injection, M4 metabolites were dominant. Supplemental Table 2 summarizes the individual percentages of radioactivity excreted in the urine and the results of urine metabolite analysis. In contrast to healthy subjects, the mean radioactivity voided into urine varied widely in patients (9.1% ± 6.9% of injected activity; range, 3.1−17.8, $n = 4$). In urine, 2 hydrophilic metabolites that eluted between 3 and 5 min on the chromatogram (U-M2, 3.5 min; M3, 4.0 min) were dominant. M3 metabolite was detected in both plasma and urine. The mean percentage of parent radioligand in voided urine in the 4 patients and 3 healthy subjects was 12.4 ± 13.4. Treatment with β-glucuronidase and sulfatase decreased the percentages of M3, and this decrease corresponded to the increases in ^{11}C-4DST percentages.

DISCUSSION

Here, we report the first clinical trial of the newly synthesized DNA synthesis marker ^{11}C-4DST for in vivo visualization of tumors.

We found ^{11}C-4DST PET to be safe and well tolerated, with no adverse effects in the 9 subjects studied. The radiation-absorbed dose was higher in the urinary bladder wall, liver, and kidney than in the other organs studied but was none-

TABLE 2

Organ Absorbed and Effective Dose Estimated from Whole-Body ^{11}C-4DST PET in Humans

Organ	Absorbed dose (μGy/MBq)
Adrenals	3.5 ± 0.1 (range, 3.4–3.5)
Brain	2.0 ± 0.1 (range, 1.9–2.1)
Breasts	2.0 ± 0.1 (range, 1.9–2.1)
Gallbladder wall	4.0 ± 0.2 (range, 3.9–4.2)
Heart wall	3.2 ± 0.2 (range, 3.0–3.5)
Kidneys	13.6 ± 3.0 (range, 10.4–16.4)
Liver	12.4 ± 2.3 (range, 10.9–15.0)
Lower large intestine wall	2.9 ± 0.1 (range, 2.8–3.0)
Lungs	2.8 ± 0.6 (range, 2.2–3.4)
Muscle	2.4 ± 0.1 (range, 2.3–2.5)
Osteogenic cells	4.7 ± 0.2 (range, 4.4–4.9)
Ovaries	3.0 ± 0.1 (range, 2.9–3.1)
Pancreas	3.4 ± 0.0 (range, 3.4–3.4)
Red marrow	4.5 ± 0.6 (range, 3.9–5.0)
Skin	1.9 ± 0.1 (range, 1.8–2.0)
Small intestine	3.9 ± 0.3 (range, 3.6–4.2)
Spleen	6.9 ± 1.4 (range, 5.5–8.2)
Stomach wall	2.8 ± 0.1 (range, 2.7–2.9)
Testes	2.3 ± 0.1 (range, 2.2–2.4)
Thymus	2.4 ± 0.1 (range, 2.3–2.5)
Thyroid	2.3 ± 0.1 (range, 2.1–2.4)
Upper large intestine wall	3.0 ± 0.1 (range, 2.9–3.1)
Urinary bladder wall	17.6 ± 2.7 (range, 15.3–20.6)
Uterus	3.4 ± 0.0 (range, 3.4–3.4)
Total body	2.8 ± 0.0 (range, 2.8–2.8)

Data are mean ± SD and range for healthy subjects ($n = 3$). Effective dose is 4.2 ± 0.3 (range, 4.0–4.5) μSv/MBq.

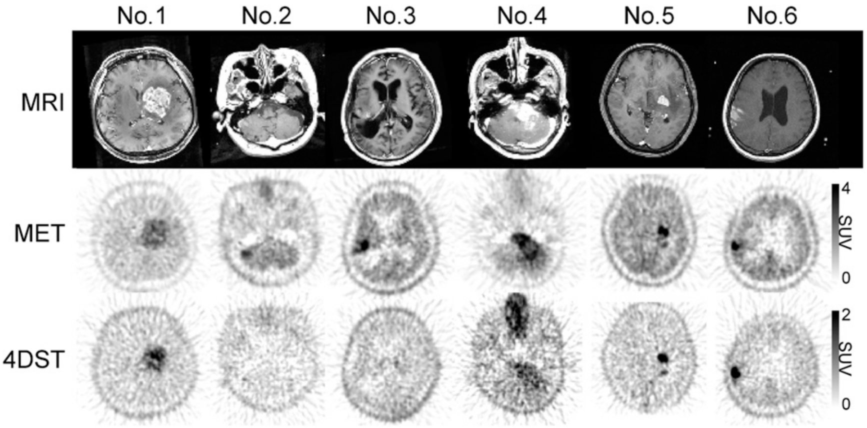

FIGURE 3. Gd-MRI, ^{11}C-methionine PET, and ^{11}C-4DST PET of 6 patients. Patient numbers correspond to those in Table 1. Gd-MRI shows evidence of blood–brain barrier disruption and gives anatomic references for PET. In ^{11}C-methionine (MET) PET images, SUV is summed for 20–40 min. In ^{11}C-4DST PET images, SUV is summed for 45–60 min for subjects 2−4 and subject 6, for 30–45 min for subject 1, and for 30–40 min for subject 5.

theless sufficiently low for clinical use. The individual-organ and total-body doses associated with ^{11}C-4DST PET were lower than those of 3′-deoxy-3′-^{18}F-fluorothymidine (*21*). This lower level of radiation burden is beneficial when performing PET serially to assess tumor response to therapy.

Human whole-body imaging showed relatively low background levels of radioactivity in the head and neck, thorax, lower abdomen, and extremities. Thus, ^{11}C-4DST PET may be useful for the detection of head and neck tumors, lung tumors, abdominal tumors, and sarcomas. In contrast to the significant myocardial uptake of ^{11}C-thymidine and ^{18}F-labeled 1-(2′-deoxy-2′-fluoro-beta-D-arabinofuranosyl)-thymine) (*2*), ^{11}C-4DST showed low uptake in the heart wall, reflecting its low affinity for thymidine kinase 2, a mitochondrial isozyme that is present at relatively high levels in the human heart and is not related to cellular proliferation. Because ^{11}C-4DST can readily image the marrow and liver, detection of tumors in this location will be limited.

There was a large difference between the systemic pharmacokinetics and distribution of ^{11}C-4DST found in humans and previous findings in mice (*10*); although stable in mice, ^{11}C-4DST was metabolized in the human body. This represents a limitation of ^{11}C-4DST for routine clinical use. Metabolite analysis indicated that some amount of ^{11}C-4DST was glucuronidated in the human body. The presence of a radioactive glucuronidated metabolite was consistent with the high uptake of radioactivity in the human liver, which is inconsistent with the low uptake in the mouse liver (*10*).

In this preliminary trial, we could not identify the trapping mechanisms of ^{11}C-4DST. Time–activity curves in the proliferating tissues and tumors showed retention, and *K*i showed a linear increase. Radioactivity retention and the linear increase in *K*i do not indicate whether images were the result of sustained delivery and transport of the tracer, metabolic trapping as a phosphorylated form, or DNA synthesis. To address these important questions, understanding the rate-limiting step for tissue retention of 4DST is necessary. Especially, understanding the rate of cellular transport, nucleoside phosphorylation, DNA trapping of labeled nucleotides, and loss of radioactivity from nucleotide dephosphorylation is the critical point.

The most important application of cell proliferation imaging is the monitoring of cancer treatment response. Interestingly, in subject 3, who received 1 course of treatment with temozolomide 3 d before PET examination, the level of ^{11}C-4DST uptake was negligible in the tumor regions where high uptake of ^{11}C-methionine was observed on the same day (Fig. 3). The enhanced tumor mass in this subject remained unchanged for 6 mo after commencement of treatment with temozolomide. In contrast, in subject 1, who also received temozolomide, rapid and high-level ^{11}C-4DST uptake was observed in the tumor region (Fig. 3). The tumor in this patient showed progressive enlargement despite continuous treatment with temozolomide. These observations suggested that cell proliferation in the tumor had been suspended by temozolomide treatment in subject 3. However, this hypothesis is difficult to confirm from our

TABLE 3

Percentages of Radiolabeled Metabolites in Plasma After Intravenous Injection of ^{11}C-4DST

	M1		M2		M3		M4		M5		^{11}C-4DST	
Time (min)	Mean ± SD	*n*	Mean ± SD	*n*	Mean ± SD	*n*	Mean ± SD	*n*	Mean ± SD	*n*	Mean ± SD	*n*
3	0.6 ± 0.4	5	1.5 ± 1.3	3	1.0 ± 0.8	3	0.2 ± 0.3	5	0.1 ± 0.1	5	97.0 ± 0.6	5
10	1.4 ± 0.9	5	8.6 ± 6.5	3	1.2 ± 1.3	3	2.7 ± 4.4	5	0.1 ± 0.1	5	85.0 ± 2.4	5
20	4.0 ± 1.8	5	3.4 ± 1.8	4	14.9 ± 13.3	4	14.3 ± 14.3	5	0.9 ± 1.4	5	61.7 ± 6.9	5
30	5.4 ± 3.0	3	4.5 ± 3.3	4	5.4 ± 1.9	4	23.4 ± 18.0	5	2.2 ± 2.5	5	44.0 ± 14.6	5
40	10.0 ± 4.3	5	3.6 ± 3.0	4	7.5 ± 3.5	4	35.3 ± 13.7	5	1.6 ± 2.1	5	38.8 ± 6.8	5
60	9.9 ± 4.2	3	5.0 ± 0.9	3	5.1 ± 0.2	3	43.4 ± 11.8	4	2.5 ± 2.6	4	34.1 ± 13.6	4

preliminary observations, as no baseline scan was done and this tumor could have been a very slowly proliferating one, which might have led to little ^{11}C-4DST uptake and stable disease rather than a good treatment response.

In this study, we used Patlak graphical analysis to obtain the ^{11}C-4DST flux constant (Ki). This analysis requires the measurement of metabolite-corrected arterial blood samples in addition to a dynamic acquisition, therefore limiting the feasibility of ^{11}C-4DST PET in routine clinical settings. Our preliminary analysis showed that Ki values of ^{11}C-4DST were well correlated to SUV (Supplemental Fig. 2B). A simpler and easier alternative method to generate parametric images of ^{11}C-4DST PET is needed for routine clinical use.

CONCLUSION

The initial findings of the present study in a small group of subjects indicated that ^{11}C-4DST PET is feasible for imaging brain tumors. Dosimetry and pharmacologic safety were acceptable at the dose required for adequate PET images. To confirm whether ^{11}C-4DST PET is a useful alternative cell proliferation marker in humans, further extensive validation studies are needed.

DISCLOSURE STATEMENT

The costs of publication of this article were defrayed in part by the payment of page charges. Therefore, and solely to indicate this fact, this article is hereby marked "advertisement" in accordance with 18 USC section 1734.

ACKNOWLEDGMENTS

We thank Kunpei Hayashi, Misaki Takimoto, and Hiroko Tsukinari for technical assistance. This work was supported by Grant-in Aid for Scientific Research B 22390241 from the Japan Society for the Promotion of Science and a grant from the National Center for Global Health and Medicine. No other potential conflict of interest relevant to this article was reported.

REFERENCES

1. Toyohara J, Fujibayashi Y. Trends in nucleoside tracer for PET imaging of cell proliferation. *Nucl Med Biol.* 2003;30:681–685.
2. Bading JR, Shields AF. Imaging of cell proliferation: status and prospects. *J Nucl Med.* 2008;49(suppl):64S–80S.
3. Christman D, Crawford EJ, Friedkin M, Wolf AP. Detection of DNA synthesis in intact organisms with positron-emitting [methyl-^{11}C]thymidine. *Proc Natl Acad Sci USA.* 1972;69:988–992.
4. Mankoff DA, Schields AF, Graham MM, Link JM, Eary JF, Krohn KA. Kinetic analysis of 2-[carbon-11]thymidine PET imaging studies: compartmental model and mathematical analysis. *J Nucl Med.* 1998;39:1043–1055.
5. Mankoff DA, Shields AF, Link JM, et al. Kinetic analysis of 2-[^{11}C]thymidine PET imaging studies: validation studies. *J Nucl Med.* 1999;40:614–624.
6. Wells JM, Mankoff DA, Eary JF, et al. Kinetic analysis of 2-[^{11}C]thymidine PET imaging studies of malignant brain tumors: preliminary patient results. *Mol Imaging.* 2002;1:145–150.
7. Wells JM, Mankoff DA, Muzi M, et al. Kinetic analysis of 2-[^{11}C]thymidine PET imaging studies of malignant brain tumors: compartmental model investigation and mathematical analysis. *Mol Imaging.* 2002;1:151–159.
8. Shields AF, Grierson JR, Dohmen BM, et al. Imaging proliferation in vivo with [F-18]FLT and positron emission tomography. *Nat Med.* 1998;4:1334–1336.
9. Toyohara J, Kumata K, Fukushi K, Irie T, Suzuki K. Evaluation of [methyl-^{14}C] 4′-thiothymidine for in vivo DNA synthesis imaging. *J Nucl Med.* 2006; 47:1717–1722.
10. Toyohara J, Okada M, Toramatsu C, Suzuki K, Irie T. Feasibility studies of 4′-[methyl-^{11}C]thiothymidine as a tumor proliferation imaging agent in mice. *Nucl Med Biol.* 2008;35:67–74.
11. Toyohara J, Sakata M, Wu J, et al. Preclinical and the first clinical studies on [^{11}C]CHIBA-1001 for mapping α7 nicotinic receptors by positron emission tomography. *Ann Nucl Med.* 2009;23:301–309.
12. Sakata M, Wu J, Toyohara J, et al. Biodistribution and radiation dosimetry of the α7 nicotinic acetylcholine receptor ligand [^{11}C]CHIBA-1001 in humans. *Nucl Med Biol.* 2011;38:443–448.
13. Fujiwara T, Watanuki S, Yamamoto S, et al. Performance evaluation of a large axial field-of-view PET scanner: SET-2400W. *Ann Nucl Med.* 1997;11:307–313.
14. Meikle SR, Bailey DL, Hooper PK, et al. Simultaneous emission and transmission measurements for attenuation correction in whole-body PET. *J Nucl Med.* 1995;36:1680–1688.
15. Cristy M, Eckerman K. *Specific Absorbed Fractions of Energy at Various Ages from Internal Photons Sources.* Oak Ridge, TN: Oak Ridge National Laboratory; 1987:V1. ORNL/TM-8381.
16. Stabin MG, Sparks RB, Crowe E. OLINDA/EXM: the second-generation personal computer software for internal dose assessment in nuclear medicine. *J Nucl Med.* 2005;46:1023–1027.
17. International Commission of Radiological Protection. ICRP publication 60: 1990 recommendations of the international commission on radiological protection. *Ann ICRP.* 1991;21:493–502.
18. Nariai T, Tanaka Y, Wakimoto M, et al. Usefulness of L-[methyl-^{11}C] methionine-positron emission tomography as a biological monitoring tool in the treatment of glioma. *J Neurosurg.* 2005;103:498–507.
19. Patlak CS, Blasberg RG, Fenstermacher JD. Graphical evaluation of blood-to-brain transfer constants from multiple-time uptake data. *J Cereb Blood Flow Metab.* 1983;3:1–7.
20. Van Bocxlaer JF, Clauwaert KM, Lambert W, De Leenheer AP. Quantitative colorimetric determination of urinary p-aminophenol with an automated analyzer. *Clin Chem.* 1997;43:627–634.
21. Vesselle H, Grierson J, Peterson LM, Muzi M, Mankoff DA, Krohn KA. ^{18}F-fluorothymidine radiation dosimetry in human PET imaging studies. *J Nucl Med.* 2003;44:1482–1488.